Transport cocktails for cancer therapeutics

Michail E. Kavousanakis,[1] Omkar Bhatavdekar,[2] Remco Bastiaannet,[3] Yannis Kevrekidis,[2,*] and Stavroula Sofou[2,†]

[1]*School of Chemical Engineering, National Technical University of Athens, Athens 15780, Greece*

[2]*Department of Chemical and Biomolecular Engineering, Institute for NanoBioTechnology, Johns Hopkins University, Baltimore, Maryland 21218, USA*

[3]*Department of Radiology and Radiological Science, School of Medicine, Johns Hopkins University, Baltimore, Maryland 21287, USA*

(Received 22 March 2024; accepted 10 July 2024; published 5 August 2024)

Beyond biological cell heterogeneity, evidenced by different resistances to therapeutics, "delivery heterogeneity" crucially limits treatment efficacy for advanced solid tumors: variations in therapeutic drug delivery to different tumor areas (perivascular, perinecrotic) leading to nonuniform drug concentrations/doses and to unsuccessful treatment (cancer cell kill). Short-range (40–80 μm), high energy (1–5 MeV) α particles successfully address the biological heterogeneity: the double-strand DNA breaks they cause make them impervious to cell resistance mechanisms. Multiresponsive nanocarriers and/or engineered antibody-drug-conjugates are elegant approaches to delivering such α-particle emitters. Delivery heterogeneity, however, remains a challenge in established (i.e., large, vascularized) tumors. Remarkably, delivery properties enabling efficacy at the cell scale (targeting selectivity, affinity, cell drug uptake) may act against spatial delivery uniformity at the tumor scale (binding-site barrier effect). We have previously demonstrated, in different mouse models, that spatial delivery uniformity, key to the effective killing of solid tumors, can be achieved utilizing combinations of different, distinct delivery carriers of the same emitter, but with different, complementary delivery properties, "leaving no cancer cell behind." We build first principles reaction-transport models (quantitatively informed by experiments) that explain the "geographically complementary" behaviors of such carrier cocktails, and help optimally design these cocktails and their delivery protocols.

DOI: 10.1103/PhysRevResearch.6.033137

I. INTRODUCTION

Although cancer death rates are decreasing, mainly due to early detection, cases of advanced metastatic and/or recurrent solid cancers still have no cure [1]. At the advanced stage of established (i.e., large, vascularized) tumors, current therapeutic approaches necessarily resort to combinations of therapeutics [2]; unfortunately, even with highly toxic combination regimens, the vast majority of patients fail to reach a durable response. A major reason for this outcome is the heterogeneity in drug delivery within established solid tumors [3–5]. Most therapeutic agents require being physically present in the vicinity of their molecular target in order to act. The limited penetration into solid tumors of nanocarriers and/or of targeting antibody-drug-conjugates, inevitably leave tumor regions exposed to too low or nonlethal levels of therapeutics, ultimately enabling disease recurrence [3,6–8]. A treatment strategy addressing delivery heterogeneities in established lesions is critical to successfully treating solid tumor patients especially at advanced stages of their disease.

This work is motivated by the *in vivo* observations in Fig. 1 [4,9]. The three-dimensional (3D) diagram quantifies how, and the representative α-camera snapshots above it partially explain why, delivery of the same injected radioactivity to vascularized solid tumors in mice is markedly more successful in inhibiting tumor growth when split in equal parts between two separate and distinct carriers: approximately 50% via targeting antibodies and ∼50% via tumor-responsive liposomes. Compared to the same total injected radioactivity delivered either (a) 100% via antibodies, or (b) 100% via liposomes, the carrier "cocktail" performs quantifiably better. The images in Fig. 1 strongly suggest that this improvement is due to the better tissue penetration of α particles delivered via the carrier cocktail, in stark contrast to the nonuniformity observed with either pure carrier.

We set out to quantitatively model these nonintuitive results through first-principles modeling of the transport and kinetic processes involved in the drug delivery process; the kinetic and transport parameters in the mathematical model were arrived at via targeted experiments.

Our two separate carriers have complementary delivery properties: one acting at the cell scale (antibody targeting) and the other acting at the tumor scale (liposome content release). Each carrier type preferentially kills a different region

*Contact author: yannisk@jhu.edu
†Contact author: ssofou1@jhu.edu

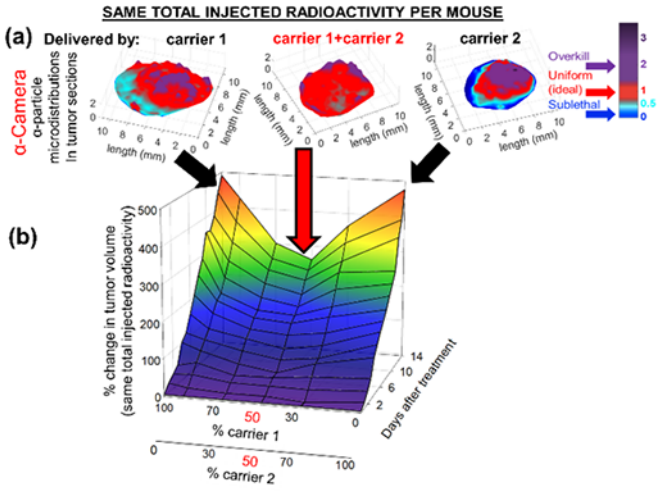

FIG. 1. Improved drug spreading within solid tumors using simultaneously two separate delivery carriers. To improve drug spreading within solid tumors, two separate delivery carriers *of the same drug*, were employed. The carriers were chosen to deliver their therapeutic cargo in complementary regions of the same solid tumor. Collectively, the drug became more well spread within established, soft-tissue solid tumors, resulting in better tumor growth inhibition. (a) Top panel: Spatial microlandscapes (color maps) exhibiting the deviation from uniform irradiation of tumor sections. α-camera images of tumor sections, where pixel intensities of delivered radioactivity were divided by the mean intensity, which was averaged over the entire tumor section, with the aim to reveal deviation from the mean (colored vertical bar). On tumor sections, local α-particle activities that were similar to the mean tumor uptake were colored in red [4]. (b) 3D-plot: Tumor growth inhibition was greater when the same total administered activity was equally split between the two separate carriers [9], even though the tumor absorbed dose at 50:50 split (0.23 ± 0.02 Gy) was lower than the dose (0.34 ± 0.04 Gy) delivered by the radiolabeled targeting antibody alone (100% carrier 2).

of the tumor [4,9]: (1) the tumor-responsive liposomes, that, on tumor uptake, release in the interstitium a highly diffusing form of their payload, which then penetrates the deeper parts of tumors where antibodies do not reach, and (2) the separately administered, less-penetrating drug or isotope-labeled targeting antibody, that effectively kills the tumor perivascular regions from where the liposomes released contents clear too fast.

Our tumor-responsive liposomes are composed of membranes forming phase-separated lipid domains (resembling lipid patches) with lowering pH [10,11]. During circulation in the blood, such liposomes comprise well-mixed, uniform membranes that stably retain their encapsulated contents. In the acidic tumor interstitium (pH $\sim$ 6.5–6.7) lipid-phase separation results in formation of *lipid patches (rafts)* that span the bilayer, creating transient lipid-packing defects along the patch boundaries, and enabling release of encapsulated agents. The liposomes may also exhibit an adhesive property that enables them to bind to the tumors' extracellular matrix, delaying their clearance from tumors [6,8].

The antibody-isotope-conjugates utilized herein comprise FDA-approved antibodies, which are designed to stably retain their therapeutic cargo [4,9,12]. These conjugates exhibit strong binding to cell surface markers and become internalized. Currently, α-particle radiolabeled antibody conjugates are evaluated in clinical trials against solid tumors of variable origin and over a range of targeted receptor expressions. This suggests that our cocktail approach may be broadly applicable.

In this work, we develop and implement an experimentally informed mathematical model that can ultimately predict the best possible combinations of the two carriers for given tumor sizes. Intratumoral spatiotemporal profiles of the therapeutic agents, delivered by each carrier type, and the corresponding intratumoral delivered radioactivity are calculated, so as to identify the optimal delivery modality combination including the associated temporal dosing scheduling.

II. RESULTS

We develop experimentally informed reaction-diffusion models to describe isotope delivery jointly from both isotope-releasing liposomes [Eqs. (2)–(5)] and antibodies [Eqs. (6)–(9)]. Each model component succinctly captures the distinct transport characteristics of its respective carrier:

(a) Tumor-responsive (due to tumor acidity) liposomes release their payload, which can reach the deeper parts of tumors.

(b) Isotope-labeled antibodies, though less penetrating, exhibit highly effective tumor cell elimination, particularly in the perivascular areas.

Finally, we systematically explore the optimal synergy between these carriers, tailoring them to specific tumor sizes.

A. Modelling tumor-responsive liposome isotope delivery

For our simulations, we assume a specific activity 0.34 MBq/μmol lipid [9]. Considering the half-life of ^{225}Ac, $t_{1/2} =$ 9.9 d, and that each decay of ^{225}Ac generates four α particles and three radioactive daughters [13], the radioactivity of ^{225}Ac is $\sim$2000 MBq/nmol of isotope. Thus, the ratio of isotope content per liposome (considering 100 000 lipids per liposome) is equal to $N_c \approx 0.017$ mol ^{225}Ac atom per mol liposome. In addition, we assume an apparent diffusion coefficient for the released isotope equal to, $D_C = 2 \times 10^{-11}$ m^2 s^{-1} (see Sec. IV D 2). To obtain the spheroid volume fraction that is accessible to isotope, ϕ_C, we estimate the volume of the spheroid unoccupied by cancer cells. With a mean diameter of 10 μm per cancer cell, in a spheroid of radius $\sim$200 μm, that consists of $\sim$16 400 cancer cells, we estimate $\phi_C \approx 0.73$.

We simulate the incubation of tumor spheroids in a solution of liposome concentration, $[L^{(\mathrm{sol})}] = 30$ μM for 6 h and compute the isotope concentration during isotope uptake, and then during the first 4 h on the completion of incubation (clearance experiments). The parameter values for the liposome-carriers simulation are as follows: the effective diffusion coefficient of liposomes in the spheroid, $D_L = 1.5 \times 10^{-13}$ m^2 s^{-1}; the mass transfer coefficient for liposomes during uptake and clearance experiments, respectively: $P_{L,\mathrm{up}} = 1.9 \times 10^{-9}$ m s^{-1}, $P_{L,\mathrm{cl}} = 5.8 \times 10^{-9}$ m s^{-1}. These parameter values, used in the simulations, are derived by fitting the model to targeted experiments described in Sec. IV D 2. The

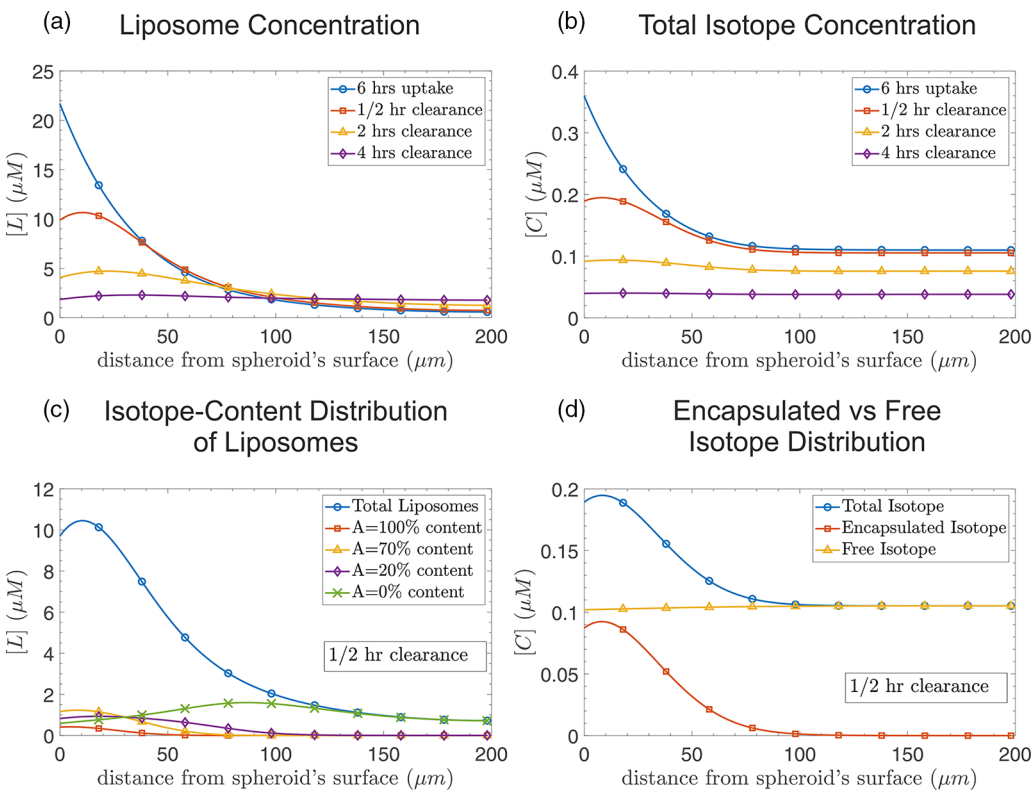

FIG. 2. Representative liposome isotope carrier simulation results. (a) Spatial distribution of liposomes in a tumor spheroid at the end of incubation (6 h: blue line with open circles), 1/2 h after incubation (red line with open squares), 2 h after incubation (yellow line with open triangles), and 4 h after incubation (purple line with open diamonds). (b) Isotope concentration spatial distribution at the end of incubation (blue line with open circles), and 1/2, 2, 4 h after the completion of incubation depicted with red line and open squares, yellow line and open triangles, and purple line with open diamonds, respectively. (c) Distribution of liposomes depending on their isotope content, A, 1/2 h after the completion of the 6-h incubation experiment. The total concentration of liposomes is depicted with a blue line with open circles; liposomes with $A = 100, 70, 20\%$ isotope content are shown with red line and open squares, yellow line and open triangles, and purple line with open diamonds, respectively. Liposomes already empty of isotope ($\sim$0% content) are denoted with the crossed green line. (d) The total isotope concentration spatial distribution 1/2 h after the completion of incubation is shown as a blue line and open circles. The encapsulated isotope in the liposomes is depicted with the red line and open rectangles, while isotope released in the interstitium is illustrated with the yellow line and open triangles. Tumor spheroids are incubated for 6 h in a solution of liposome concentration, $[L^{(\mathrm{sol})}] = 30$ μM. Parameter values for the simulation: the effective diffusion coefficient of liposomes in the spheroid, $D_L = 1.5 \times 10^{-13}$ m^2 s^{-1}; the mass transfer coefficient for liposomes during uptake and clearance, respectively: $P_{L,\mathrm{up}} = 1.9 \times 10^{-9}$ m s^{-1}, $P_{L,\mathrm{cl}} = 5.8 \times 10^{-9}$ m s^{-1}; the apparent diffusion coefficient of the isotope, $D_C = 2 \times 10^{-11}$ m^2 s^{-1}, and the isotopes mass transfer coefficients, $P_{C,\mathrm{up}} = 1.7 \times 10^{-8}$ m s^{-1} and $P_{C,\mathrm{cl}} = 2.9 \times 10^{-8}$ m s^{-1}, respectively.

same set of parameter values is then used for the cocktail simulations.

Liposomes release their isotope content at a rate dependent on pH; in particular, the release rate constant, k_r, has been experimentally measured to correlate with pH in a linear fashion, $k_r = a + b \cdot$ pH. For the purpose of our simulations, we compute the values of constants, a and b by fitting the isotope release kinetics of liposomes when loaded with a drug-surrogate (see Supplemental Material, Sec. B [14]), and obtain the following simple empirical relation:

$$k_r = 0.48 - 0.064 \cdot \text{ pH min}^{-1}. \tag{1}$$

Importantly, experimental measurements show a spatial variation of pH within a growing spheroid. Figure (S-1) of the Supplemental Material [14] depicts the pH variation in BT-474 spheroids with the distance from the spheroid's center. The environment in the tumor's interior is more acidic, implying higher drug-release rates [see Eq. (1)], compared to the exterior regions of the spheroid.

Figure 2(a) shows different temporal snapshots of the spatial distribution of liposome concentration within a spheroid following incubation. Liposomes diffuse and manage to penetrate the spheroid up to certain depths during the incubation stage. Even on completion of isotope uptake, liposomes can still be found at the interior of the spheroid; these are mostly liposomes that have already released all their isotope-content [see Fig. 2(c)]. Liposomes will gradually release their isotope as they diffuse towards the interior of the spheroid (and the environment becomes more acidic); one can thus observe higher concentration of lower-content liposomes closer to the tumor's center. We compute the distribution of isotope, carried and released by the liposomes, during incubation or uptake as well as during clearance phases with respect to the spheroids [Fig. 2(b)]. The isotope is released by the liposomes and diffuses quickly towards the interior region of the spheroid,

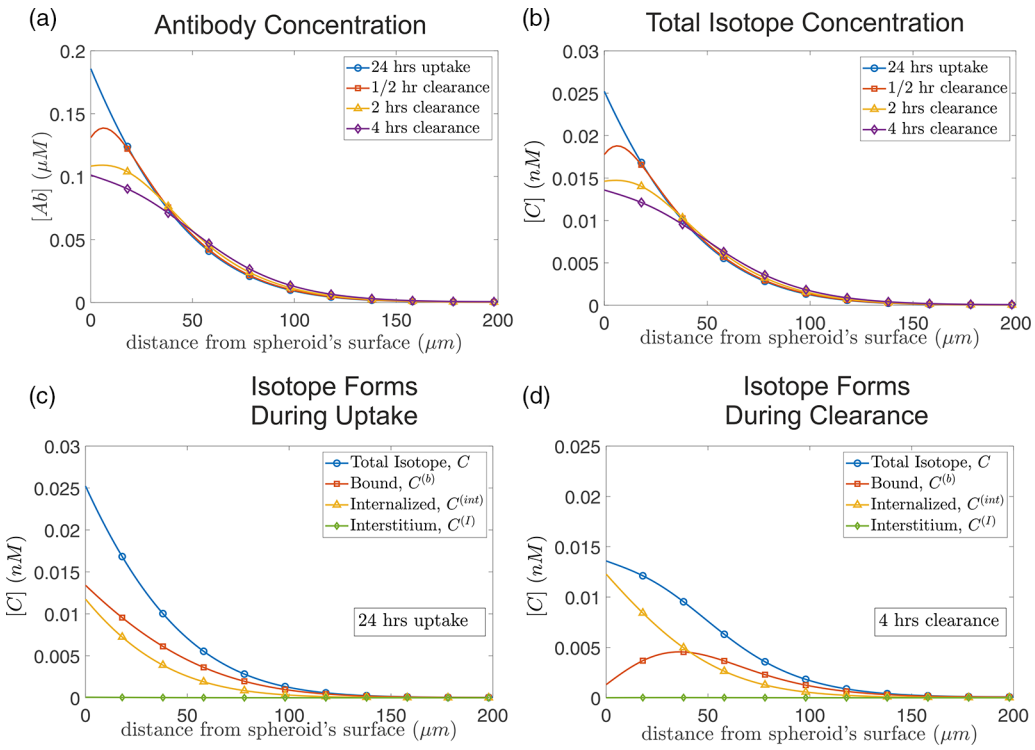

FIG. 3. Antibodies isotope carrier simulation. (a) Spatial distribution of antibody-isotope complexes within a tumor spheroid at the end of incubation (24 h: blue line with open circles), 1/2 h after incubation (red line with open squares), 2 h after incubation (yellow line with open triangles), and 4 h after incubation (purple line with open diamonds). (b) Isotope concentration spatial distribution at the end of incubation (blue line with open circles), and 1/2, 2, 4 h after the completion of incubation depicted with red line and open squares, yellow line and open triangles, and purple line with open diamonds, respectively. (c) Spatial distribution of isotope concentration after the completion of the 24 h incubation experiment. The total isotope concentration is depicted with a blue line with open circles; receptor-bound isotope concentration is shown in red line and open squares. The internalized isotope concentration is depicted with yellow line and open triangles; and the isotope found in the interstitium is illustrated with the green line with open diamonds. The corresponding profiles of the various forms of isotope during clearance, and specifically 4 h after the completion of incubation, are depicted in (d). Parameter values for the simulation: $D_{Ab} = 6 \times 10^{-12}$ $m^2\,s^{-1}$, $K_D = 5$ nM, $k_{off} = 4 \times 10^{-3}$ s^{-1}, $k_{int} = 1.4 \times 10^{-5}$ s^{-1}, $P_{Ab,up} = 2.5 \times 10^{-10}$ $m\,s^{-1}$, $P_{Ab,cl} = 8 \times 10^{-7}$ $m\,s^{-1}$, and $R_T = 1060$ nM. The simulations are performed considering a fixed concentration of antibodies in the solution where antibodies are immersed during incubation: $[Ab^{(sol)}] = 240$ nM.

where it remains even after the completion of incubation. Figure 2(d) shows the uniform distribution of the released -by the liposomes- isotope (in its free form). Higher concentration is observed at the outer region of the spheroid, where liposomes with higher isotope content can be found.

B. Modelling antibody isotope delivery

Tumor spheroids are incubated in a solution of constant antibody for 24 h in silico, as in experimental practice. Antibodies then penetrate the spheroid, bind on the cancer cells, and gradually become internalized by them. We simulate these processes by numerically solving model Eqs. (6)–(9) below. We consider a constant concentration of antibodies in the solution where spheroids are immersed; during the uptake experiments, which last 24 h, the concentration of antibodies in the incubating solution is fixed to $[Ab^{(sol)}] = 240$ nM. If we assume a specific activity 1.87 MBq/mg Ab [9] (here the antibody is Trastuzumab with molecular weight 150 kDa), then the ratio of isotope per Ab is approximately 1.45×10^{-4} mol isotope/mol Ab (as reported above the radioactivity for ^{225}Ac is approximately 2000 MBq/nmol isotope). For our simulations, we adopt the following set of parameter values: the effective diffusion coefficient of antibodies in the spheroid: $D_{Ab} = 6 \times 10^{-12}$ $m^2\,s^{-1}$; the equilibrium dissociation constant for antibodies: $K_D \equiv k_{off}/k_{on} = 5$ nM; the dissociation rate constant: $k_{off} = 4 \times 10^{-3}$ s^{-1}; the internalization rate constant: $k_{int} = 1.4 \times 10^{-5}$ s^{-1}; the mass transfer coefficient for antibodies during uptake and clearance experiments, respectively: $P_{Ab,up} = 2.5 \times 10^{-10}$ $m\,s^{-1}$, $P_{Ab,cl} = 8 \times 10^{-7}$ $m\,s^{-1}$; the concentration of unoccupied by antibodies receptors: $R_T = 1060$ nM. These values are derived from targeted experiments described in Sec. IV D 3.

Antibodies bind on the surface of cancer cells, preventing their further transport towards the interior of the spheroid (the binding-site barrier effect [15–17]). Our model predicts the spatiotemporal profiles of antibodies found in the interstitium $[Ab^{(I)}]$, the antibody-receptor complex $[Ab^{(b)}]$, and the antibody concentration $[Ab^{(int)}]$ internalized in cancer cells. Thus, one can infer the isotope concentration, given that the isotope-antibody molar ratio, as derived from the measured specific activity [4,9], is 1.45×10^{-4}. Snapshots of the total isotope concentration (denoted with C) are presented in Fig. 3(b). One can observe that the total isotope concentration does not fall

below 50% during the first 4 h of the clearance experiments; in contrast, when carried by liposomes, we observe a decay at a much higher rate [see Fig. 2(b)]. This behavior can be attributed to the antibodies binding on the cancer cell surfaces, and subsequently becoming internalized. In particular, by breaking the total isotope concentration down to its various constituent forms, we can clearly see that the isotope can mainly be found in the form of antibody-receptor complexes $[C^{(b)}]$, and in internalized antibodies $[C^{(\mathrm{int})}]$. The concentration of antibodies, and thus their isotope cargo, when they diffuse in the spheroid's interstitium, is at a substantially lower level compared to the other forms of antibodies, during both the uptake and the clearance experiments from spheroids [Fig. 3(c) and 3(d)]. Finally, we observe that the isotope concentration is practically negligible at the inner regions of the spheroid (practically negligible at distances up to 75 μm from the spheroid's center).

C. Modelling cocktail isotope delivery, jointly using liposomes as well as antibodies

As reported above, isotope delivery with tumor responsive, isotope releasing liposomes can penetrate and deliver higher values of isotope concentrations further into the spheroid's interior, whereas antibodies primarily target the exterior regions of a spheroid. It is thus reasonable to expect that the combination (cocktail) of the two carriers results in more uniform isotope distribution within spheroids. Instead of incubating spheroids in a solution with initial radioactivity concentration of 3.7 MBq/L (or equivalently ∼0.0019 nM) and transport the isotope with a single carrier (either liposomes only or antibodies only), we split the isotope to 0.00095 nM encapsulated in liposomes, and 0.00095 nM contained in antibodies. We simulate spheroid incubation with a protocol starting with antibodies for 24 h, and liposome incubation for the last 6 h of the 24. This incubation schedule is chosen to (approximately) match our knowledge of the corresponding carrier blood clearance half-lives in mice [9]; it is schematically illustrated in the right panel of Fig. 4(a). In the left and center panels of Fig. 4(a), we present the isotope distribution when administered in equal amounts utilizing both liposome and antibody carriers. The cocktail of carriers combines the increased isotope penetration capability of liposomes, and the increased concentration level of isotope that antibodies provide at the exterior regions of the spheroids. The model is augmented by a quantification of cell killing described in Sec. IV C.

By computing the isotope spatiotemporal distribution [Fig. 4(b), left panel], we can quantify the isotope's delivered (and remaining) radioactivity explicitly via the time-integral of isotope concentration [Fig. 4(b), right panel] using Eq. (12). We refer the reader to Sec. IV C in which we quantify the killing action of the isotope ^{225}Ac. In Fig. 4(c) we present the survival fraction (SF) of cancer cells' spatial distribution at time $t = 32$ h applying Eq. (12) and by setting, $k_{\mathrm{kill}} = 400\ \mathrm{nM}^{-1}\,\mathrm{h}^{-1} = 5.7 \times 10^{-11}$ L/decays. Observe that the overall treatment efficiency when the radius of spheroids is 150 μm (small spheroids) is in general higher, compared to larger size spheroids. In addition, observe the significantly higher efficiency of antibody mediated treatment in the outer regions of spheroids, which drops in the inner regions of spheroids due to the low penetration ability of antibodies. Especially in medium and large size spheroids, there exists a significant portion of the spheroid inner region where the cancer cells remain intact when the isotope is exclusively carried by antibodies. On the other hand, liposome treatment mediates the transport of isotope towards interior regions of the spheroids. Increasing the isotope dose delivered by liposomes makes treatment more effective for larger spheroids; in the absence of antibody carriers however, the therapeutic efficiency at the outer parts of the spheroids is limited. Clearly, one expects an optimum to develop.

The combined action of antibody and liposome carriers is expected to produce higher therapeutic efficacy, and in fact we quantify this through computing the average survival fraction of cancer cells. Figure 4(d) shows the relative difference of (the average) survival fraction with respect to the scheme exhibiting the best performance for small, medium, and large spheroids (left, middle, and right panel, respectively) and different combinations of antibody and liposome carriers. Antibody fraction 100% corresponds to isotope delivery exclusively using antibodies (0.0019 nM delivered with antibodies). A fraction of 50% denotes a scheme with 0.00095 nM of ^{225}Ac being delivered by antibodies and 0.00095 nM is delivered using liposomes. Finally, 0% corresponds to isotope delivery using exclusively liposomes (0.0019 nM delivered with liposomes). In all cases, the total ^{225}Ac isotope concentration in the solution at the beginning of incubation is 0.0019 nM. Optimal efficiency is achieved for 100% antibody fraction for small spheroids (150 μm radius), 40% for medium size spheroids (7.6×10^{-4} nM delivered with antibodies, 11.4×10^{-4} nM isotope delivered with liposomes), and 25% antibody fraction in larger size spheroids (4.75×10^{-4} nM delivered with antibodies, and 14.25×10^{-4} nM isotope delivered with liposomes). Clearly the model is successful in reproducing, quantifying, and mechanistically validating the initial *in vivo* observations and the intuition behind the success of transport cocktails.

III. DISCUSSION

The presented work addresses a critical challenge in the treatment of advanced solid tumors: the delivery heterogeneity of therapeutic agents within the tumor microenvironment. Beyond the intrinsic cellular heterogeneity of tumors, the delivery of therapeutic drugs to different tumor regions varies, leading to nonuniform drug concentrations and doses. By employing two distinct carriers, tumor-responsive liposomes and antibody-drug conjugates, each with complementary delivery properties, leads to improved drug spreading within solid tumors [4,6,9]. While the liposomes release their payload in the interstitium, penetrating deeper tumor regions, the antibodies target perivascular areas. Here, we integrate first-principles reaction-transport models with experimental data to elucidate the synergistic behavior of these carriers. The mathematical models, informed by experiments, successfully reproduce the geographically complementary behaviors observed in the delivery of α particles using carrier cocktails.

The study also explores the optimal synergy between the two carriers for different tumor sizes, emphasizing the importance of tailoring (optimizing) delivery protocols. The

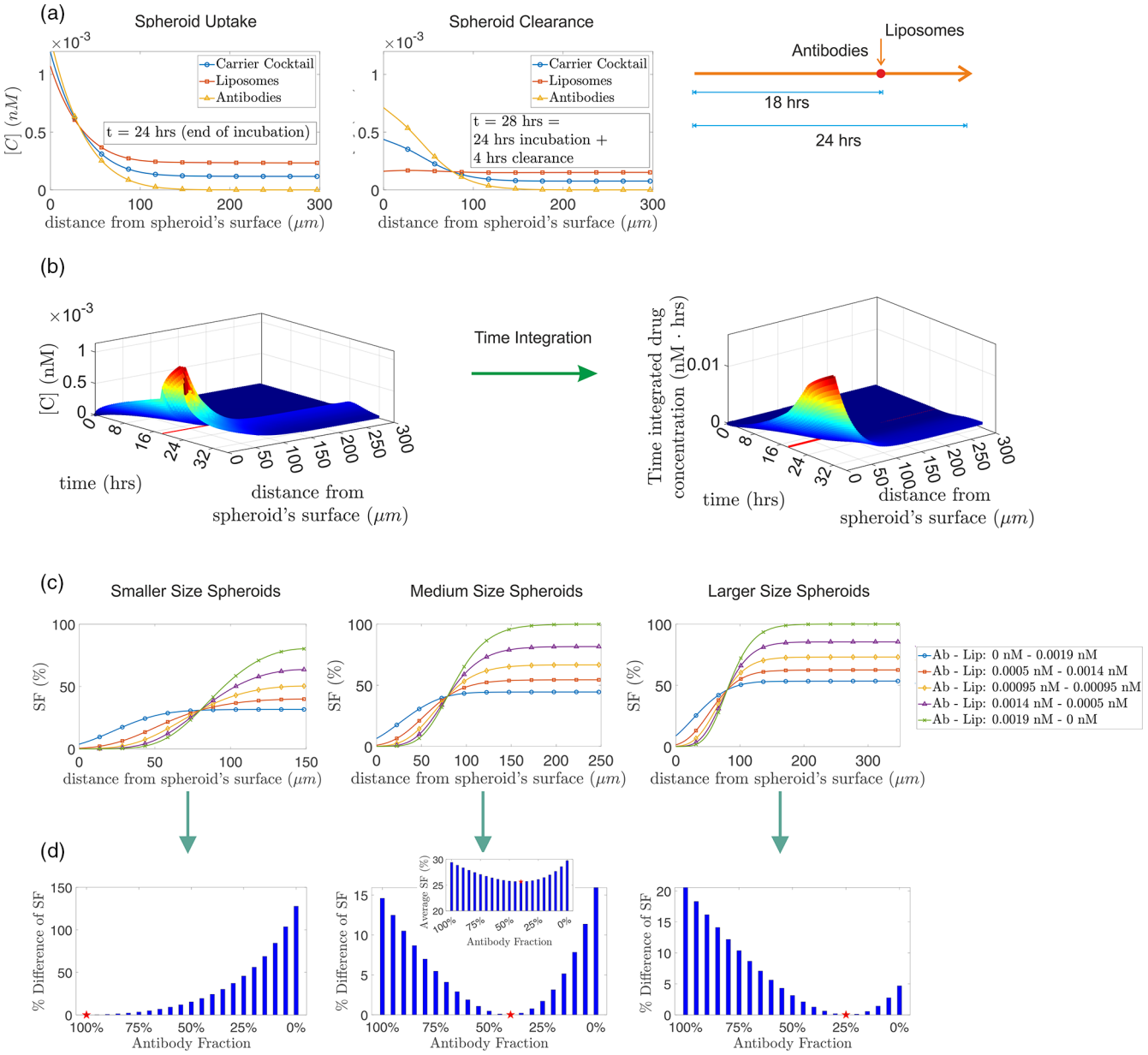

FIG. 4. Quantification of treatment efficacy for different isotope carrier combinations. (a) Comparison of isotope concentration spatial profiles obtained for different carrier cocktails. Left and middle panels illustrate profiles at the end of incubation and after 4 h of clearance time, respectively. The blue line with circles corresponds to isotope administration with a cocktail of antibody and liposome carriers; the red line with squares, and the orange line with triangles represent isotope profiles when using exclusively liposomes and antibodies, respectively. In all cases, the concentration of isotope in the solution where spheroids are immersed during uptake is 0.0019 nM. In the cocktail simulation, liposomes and antibodies cargo has a concentration of 0.00095 nM each, in the media. The right panel illustrates the isotope delivery temporal policy, with spheroids incubated in a solution of antibody isotope carriers for 24 h and liposomes injected in the solution at $t = 18$ h (total incubation time with liposome carriers= 6 h). (b) Left panel: Spatiotemporal evolution of ^{225}Ac when carried with a 50/50% combination of antibodies and liposome carriers. Spheroids are incubated in a solution of antibodies carrying 9.5×10^{-4} nM of isotope for 24 h. At $t = 18$ h liposomes carrying 9.5×10^{-4} nM of isotope are administered in the solution. The right panel depicts the time integrated isotope concentration. (c) Spatial distribution of the cancer cell SF at $t = 32$ h for different carrier combinations and different spheroid sizes. Smaller, medium, and larger spheroids have radii of 150 μm (left), 250 μm (center), and 350 μm (right), respectively. SF is computed using Eq. (12) and setting $k_{\text{kill}} = 400$ nM^{-1} h^{-1}. (d) The overall efficiency of different carrier combinations is quantified by illustrating the percentage difference in average SF relative to the most effective carrier scheme, indicated by a red star in each tumor size scenario. Higher efficiency for smaller size spheroids is attained when using exclusively antibodies (SF = 8.1%). For medium size spheroids, optimal efficiency is achieved with a 40% antibodies/60% liposomes carrier combination (SF = 25.7%). The inset shows the SF variation for different antibodies-liposomes carrier combination. For spheroids of 350 μm radius, the minimum SF = 36.8% is computed when using 75% liposomes-25% antibodies.

quantification of treatment efficacy for various carrier combinations, including exclusive use of liposomes or antibodies, highlights the superior performance of the carrier cocktail approach. The results suggest that an optimum combination of liposomes and antibodies can significantly enhance therapeutic efficacy, offering a potential solution to the delivery heterogeneity challenge in treating established solid tumors. Overall, this work provides valuable insights into the design and optimization of carrier cocktails for effective and uniform drug delivery in the complex landscape of solid tumors.

IV. METHODS

Our reaction-diffusion-type transport model consists of a set of coupled partial differential equations which describe the spatiotemporal evolution of the concentrations of various forms of each moiety (antibodies or liposomes) and the isotope they carry.

A. Isotope delivery using liposomes

When a spheroid [our surrogate of tumor avascular regions, see also right panel of Fig. 5(a)] is immersed in a solution with constant liposome concentration, then liposomes (L) are transported through diffusion in the spheroids interstitium, and release their isotope-content, C, which in turn diffuses in the spheroid interstitium [see Fig. 5(b)].

$$\frac{\partial [L]}{\partial t} = \frac{1}{r^2}\frac{\partial}{\partial r}\left(D_L r^2 \phi_L \frac{\partial}{\partial r}\left(\frac{[L]}{\phi_L}\right)\right) + \frac{\partial}{\partial A}(k_r(\mathrm{pH})\cdot[L]\cdot A). \tag{2}$$

Here $[L] = [L](A, r, t)$ denotes the liposome concentration in the interstitium, and depends on the isotope content, A, on the radial distance from the tumor spheroid center, r and of course on time, t; $k_r = k_r(\mathrm{pH})$ denotes the isotope release rate from the liposomes, and is a function of local pH. D_L is the effective diffusion coefficient of liposome in the spheroid, and ϕ_L denotes the fraction of spheroid volume accessible to liposomes.

At the spheroid's external surface, the mass flux rate is prescribed from the following mass-transfer relation:

$$D_L\phi_L \frac{\partial}{\partial r}\frac{[L](A,r,t)}{\phi_L}\Big|_{r=R} = P_{L,i}\left([L^{(\mathrm{sol})}](A) - \frac{[L](A,r,t)}{\phi_L}\Big|_{r=R}\right), \tag{3}$$

where $P_{L,i}$ is the mass transfer coefficient for liposomes during uptake (when $i = \mathrm{up}$) and during clearance when ($i = \mathrm{cl}$); $[L^{(\mathrm{sol})}](A)$ is the concentration of liposomes with isotope content A in the solution in which spheroids are immersed. R denotes the radius of the spheroid. In the solution liposomes with isotope content $A = 100\%$ are initially present.

Isotope release and transport in the spheroid is governed by:

$$\frac{\partial [C]}{\partial t} = \frac{1}{r^2}\frac{\partial}{\partial r}\left(D_C r^2 \phi_C \frac{\partial}{\partial r}\left(\frac{[C]}{\phi_C}\right)\right) + k_r(\mathrm{pH})N_C \times \int_{A=0}^{A=100\%} [L](A,r,t)\cdot A\mathrm{d}A - \frac{\log 2}{t_{1/2}}[C], \tag{4}$$

where $[C]$ is the isotope concentration in the interstitium, D_C is the effective diffusion coefficient of the isotope in the tumor interstitium, and ϕ_C denotes the fraction of spheroid accessible to isotope. N_C is the ratio of isotope content per liposome (isotope mol/liposome mol) when $A = 100\%$. In all simulations presented, this maximal isotope content per liposome is $N_C = 0.017$ moles isotope/moles liposome. Finally, $t_{1/2}$ denotes the half-life of the radioactive isotope ($t_{1/2} = 9.9$ d for ^{225}Ac). At the exterior surface of the spheroid, $r = R$, we prescribe the flux of isotope by continuity:

$$D_C\phi_C \frac{\partial}{\partial r}\frac{[C]}{\phi_C}\Big|_{r=R} = P_{C,i}\left([C^{(\mathrm{sol})}] - \frac{[C]}{\phi_C}\Big|_{r=R}\right), \tag{5}$$

where $P_{C,i}$ denotes the mass transfer coefficient for isotope from the solution to the spheroid during uptake, $i \equiv \mathrm{up}$, and during clearance, $i \equiv \mathrm{cl}$, respectively. $[C^{(\mathrm{sol})}]$ is the concentration of the free isotope in the solution where the spheroids are immersed. Since the solution initially contains only isotope encapsulated by liposomes, $[C^{(\mathrm{sol})}](t = 0) = 0$, and we assume here that, for a large bath, it remains practically negligible during incubation.

B. Isotope delivery using specific antibodies

When a spheroid is immersed in a solution with constant antibody concentration, antibodies enter the spheroid through the outer tumor surface. Once in the tumor interstitium, antibodies are transported by diffusion, bind with surface receptors, dissociate from them, and/or become internalized within the cells [see Fig. 5(c)]. Again, we formulate reaction-diffusion equations that describe the processes involved, and in particular:

$$\frac{\partial [Ab^{(I)}]}{\partial t} = \frac{1}{r^2}\frac{\partial}{\partial r}\left(D_{Ab} r^2 \phi_{Ab}\frac{\partial}{\partial r}\left(\frac{[Ab^{(I)}]}{\phi_{Ab}}\right)\right) - k_{\mathrm{on}}\frac{[Ab^{(I)}]}{\phi_{Ab}}R_f + k_{\mathrm{off}}[Ab^{(b)}], \tag{6}$$

$$\frac{\partial [Ab^{(b)}]}{\partial t} = k_{\mathrm{on}}\frac{[Ab^{(I)}]}{\phi_{Ab}}R_f - k_{\mathrm{off}}[Ab^{(b)}] - k_{\mathrm{int}}[Ab^{(b)}], \tag{7}$$

$$\frac{\partial [Ab^{(\mathrm{int})}]}{\partial t} = k_{\mathrm{int}}[Ab^{(b)}], \tag{8}$$

where $[Ab^{(I)}]$ denotes the antibody concentration in the interstitium, $[Ab^{(b)}]$ is the concentration of the antibody-receptor complex, and $[Ab^{(\mathrm{int})}]$ denotes the concentration of internalized antibody; D_{Ab} denotes the effective diffusion coefficient of antibodies when transported in the interstitium; k_{on}, k_{off} denote the association and dissociation rate constants on or from the cell surface, respectively and k_{int} is the internalization rate constant; R_f is the concentration of unoccupied (by antibodies) receptors, and ϕ_{Ab} is the fraction of spheroid volume accessible to antibody.

The mass flux rate at the spheroid's external surface is given by:

$$D_{Ab}\phi_{Ab}\frac{\partial}{\partial r}\left(\frac{[Ab^{(I)}]}{\phi_{Ab}}\right)\Big|_{r=R} = P_{Ab,i}\left([Ab^{(\mathrm{sol})}] - \left(\frac{[Ab^{(I)}]}{\phi_{Ab}}\right)\Big|_{r=R}\right), \tag{9}$$

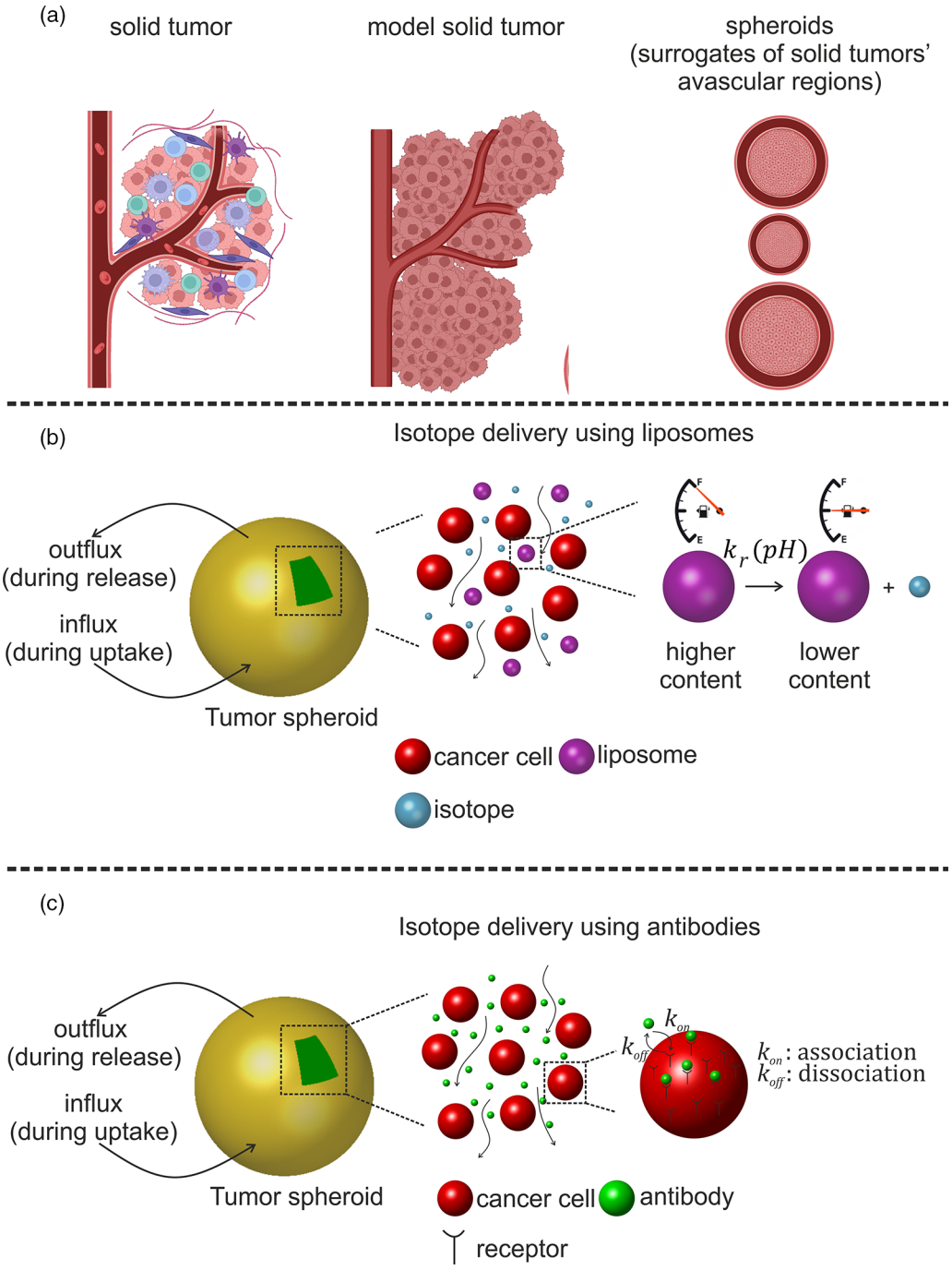

FIG. 5. (a) Schematic representation of a solid tumor that is approximated as a "composite" material comprising the tumor's (neo)vasculature and avascular regions, which are rich in cancer cells. The blood vessel–to–blood vessel distances vary, and the multicellular spheroids are surrogates of these avascular tumor regions. The "edge" of the spheroids essentially coincides with the solid tumor's neovasculature wall or boundary. A solid tumor is simply approximated as an "agglomerate" of spheroids of different sizes with (neo)vasculature at their interfaces. (a) Drawing created using BioRender. [(b) and (c)] Schematic representation of processes involved during uptake and clearance experiments of isotope-carriers to a spheroid. (b) When the isotope-carriers are liposomes, they infiltrate the spheroid, and release their isotope content with a pH dependent rate constant, k_r(pH). (c) When antibodies are used as isotope-carriers, they diffuse through the interstitium of the tumor and associate (dissociate) on (from) the cancer cell surface at rate constants k_{on}, k_{off}, respectively.

where $[Ab^{(\text{sol})}]$ is the antibody concentration in the solution in which spheroids are immersed, and $P_{Ab,i}$ denotes the mass transfer coefficient, equal to $P_{Ab,\text{up}}$ for uptake experiments, and $P_{Ab,\text{cl}}$ for clearance experiments. Finally, we consider the following material balance for surface receptors:

$$[Ab^{(b)}] + R_f = R_T = \text{const}, \tag{10}$$

with R_T denoting the initial (unbound) receptor concentration. All concentrations are expressed over the total spheroid volume (both accessible and inaccessible to antibodies).

C. Killing efficacy

The cargo-isotope is an α-particle generator which can result in high cancer-cell killing with minimal irradiation. Here, we consider ^{225}Ac which decays with a 9.9-d half-life, generating a total of four α particles, with range in tissue between 40 and 80 μm (5–10 cell diameters), and three radioactive daughters [13]. Without loss of generality, the decay of radioactive daughters is assumed to occur in the vicinity of the parent ^{225}Ac nucleus. In this study, we assume that the death kinetics of the cancer cells in the spheroid follow:

$$\frac{\mathrm{d}T}{\mathrm{d}t} = -k_{\mathrm{kill}}[C]T = -\tilde{k}_{\mathrm{kill}}\dot{D}T, \tag{11}$$

where $T(r,t)$ denotes the density of surviving cancer cells at radial distance, r, from the center of and time, t, $[C]$ is the local concentration of ^{225}Ac, and k_{kill} denotes the killing rate constant of cancer cells ($\tilde{k}_{\mathrm{kill}}$ when death kinetics are expressed in terms of decay rate, $\dot{D}$). The concentration of ^{225}Ac isotope can be correlated with its decay rate, given the half-life of the isotope, $t_{1/2} = 9.9$ d, and that each decay generates four α particles and three radio-active daughters [13]. The radioactivity of ^{225}Ac is ∼2000 MBq/nmol, thus $\dot{D} \approx 2000 \times [C]$ MBq/L (when $[C]$ is expressed in nM). Then, a formula providing the survival fraction (SF) of cancer cells follows:

$$\mathrm{SF}(r,t) \equiv \frac{T(r,t)}{T(r,0)} = \exp\left(-k_{\mathrm{kill}}\int_0^t [C](r,\tau)\mathrm{d}\tau\right) = \exp\left(-\tilde{k}_{\mathrm{kill}}\int_0^t \dot{D}(r,\tau)\mathrm{d}\tau\right). \tag{12}$$

In conclusion, the killing efficiency of different isotope carrier combinations is measured by the survival fraction of cancer cells at each radial distance, r, and each time instance, t.

D. Experimentally informed parameter fitting

1. Porosity profiles

Multicellular, 3D spheroids of BT474 breast cancer cells, overexpressing the HER2-targeted marker, were formed using established methods [3], and were utilized as the surrogates of solid tumors avascular regions. The interstitial pH gradient in these spheroids was previously measured, using a fluorescent pH indicator, and was shown to range from approximately 6.5 in the core, to 7.4 at the edges, when suspended in regular media (see also Fig. (S-1) of the Supplemental Material [14]). To quantify the spatiotemporal profiles of each modality, spheroids were removed from the incubation suspension at different time points (as described in detail in references [4,6,9,12], were snap frozen, sliced, and the equatorial sections were imaged by a fluorescence microscope. The average radial intensities of each fluorescently labelled modality were calculated using an in-house erosion MATLAB code, and the radial distributions were quantified by comparing, for each fluorescent species, to calibrated curves, generated using the same microscope in a cuvette, of pathlength identical to the thickness of the spheroid sections, containing known concentrations of each fluorescent species or moiety [4,6,9,12]. For the derivation of each moiety's porosity profiles, we worked with the nonreacting or binding corresponding moieties: a nonspecific antibody, Rituximab (that was shown to not specially bind to BT-474 cells, and with nonreleasing, nonadhering liposomes (as characterized in Refs. [6–8]). Data were collected by incubating spheroids for long times (longer than 24 h) until the concentration profiles of liposomes and antibodies remained practically unaltered. In both cases, the steady-state solution of the model [see Eqs. (2) and (6)] must be a uniform solution, and in particular: $[L]^{(\mathrm{steady})}(r) = \phi_L[L^{(\mathrm{sol})}]$ and $[Ab]^{(\mathrm{steady})}(r) = \phi_{Ab}[Ab^{(\mathrm{sol})}]$ for liposomes and antibodies, respectively. Thus, one could infer the porosity profile by fitting curves $\phi_L(r)$, $\phi_{Ab}(r)$ to the data, $[L]/[L^{(\mathrm{sol})}]$ and $[Ab^{(I)}]/[Ab^{(\mathrm{sol})}]$ [see Figs. 6(a) and 6(b)]. For the computation of porosity profile, spheroids were incubated with "drug or isotope-empty," nonadhering liposomes, and nonspecific, nonassociating antibodies Rituximab ($k_{\mathrm{on}} = k_{\mathrm{off}} = 0$, see Eq. (6) in Sec. IV). The resulting porosity fitting for nonadhering, nonreleasing liposomes is: $\phi_L \approx 0.44r^{3.2} + 0.56$, and for nonspecific antibodies: $\phi_{Ab} \approx 0.83r^{5.21} + 0.17$. The porosity profile for liposomes features larger variation (compared to antibodies), with considerably lower values at the spheroid's center; at the center of a spheroid only ∼17% of the volume is accessible to liposomes.

2. Obtaining transport parameters for nonadhering, nonreleasing liposomes

Estimation of transport parameters, D_L, and $P_{L,\mathrm{up(cl)}}$ is performed by fitting the continuum model [Eqs. (2) and (3)] to experimental measurements of liposomal radial distributions during uptake and clearance experiments. We simulate the spatiotemporal evolution of nonadhering, nonreleasing, isotope-free liposomal carriers, which simplifies our computations. The experimental data are obtained by incubating spheroids in a solution of concentration, $[L^{(\mathrm{sol})}] = 0.5$ mM liposomes for 6 h; then spheroids are fished from the medium and are immersed in clear media (clearance) for another 24 h. Figure 6(c) illustrates the best fitting simulation of the continuum model, Eqs. (2) and (3) on experimental measurements of nonadhering, nonreleasing liposomes. Best fits are obtained using MATLAB's function *nlnfit*, which performs nonlinear regression using iterative least squares estimation. The estimated effective diffusion coefficient of liposomes in the spheroids is: $D_L = (1.46 \pm 0.13) \times 10^{-13}$ m^2 s^{-1}. The mass transfer coefficient of liposomes during incubation is estimated as: $P_{L,\mathrm{up}} = (1.91 \pm 0.18) \times 10^{-9}$ m s^{-1}. The mass transfer coefficient of liposomes during clearance experiments (spheroids immersed in clean water) is estimated: $P_{L,\mathrm{cl}} = (5.81 \pm 1.0) \times 10^{-9}$ m s^{-1}.

Similarly, to estimate the diffusion coefficient and mass transfer coefficients of the drug released from liposomes within the interstitium, spheroids were incubated with 3 μM free Newport Green (NG) for up to 6 h and were sampled both during the uptake and clearance of NG, at different time points. The spatiotemporal distributions of NG within spheroids were quantified and were analyzed as described above for liposomes. The diffusion coefficient for NG is estimated: $D_C = (1.96 \pm 0.19) \times 10^{-11}$ m^2 s^{-1}, the

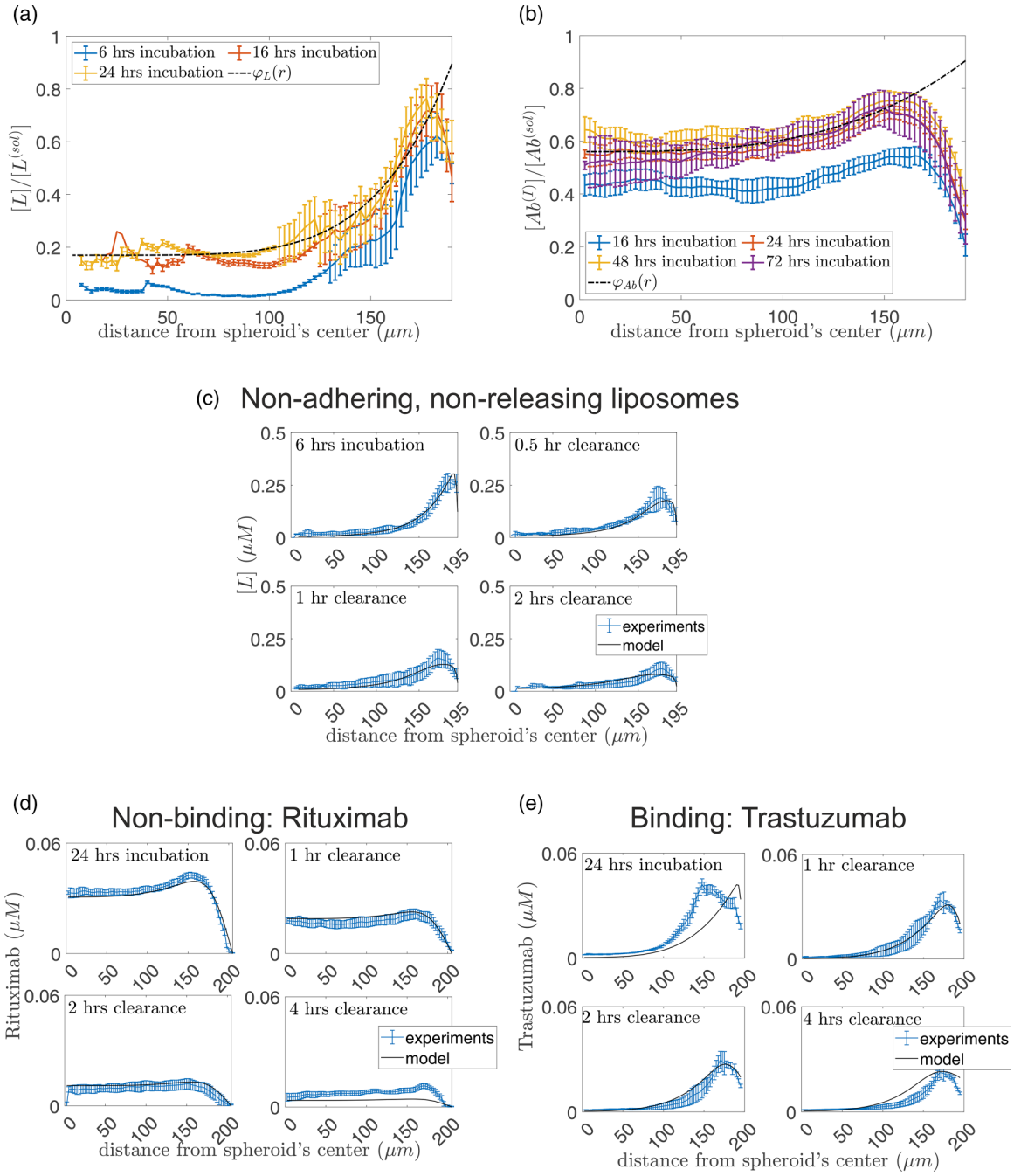

FIG. 6. Fitting of transport and kinetic properties. (a) Porosity profile for nonadhering liposomes. (b) Porosity profile for nonbinding antibodies. (c) Fitting of transport properties on nonreleasing, nonadhering liposomes uptake and clearance experiments. (d) Fitting of transport properties on nonbinding, Rituximab antibody experiments (uptake and clearance). (e) Fitting of kinetic properties on binding or specific Trastuzumab antibodies experiments.

drug mass transfer coefficient during uptake and clearance: $P_{C,\mathrm{up}} = (1.7 \pm 0.01) \times 10^{-8}$ m s^{-1} and $P_{C,\mathrm{cl}} = (2.9 \pm 0.2) \times 10^{-8}$ m s^{-1}, respectively. Assuming that the mass transport property values of NG are similar to those of the isotope, we incorporate them into our computations.

3. *Transport and kinetic parameters for antibodies*

We first estimate transport properties of antibodies by fitting Eqs. (6)–(9) to experimental data of nonbinding antibodies (Rituximab). Tumor spheroids are immersed in a 0.06 μM Rituximab solution for 24 h (incubation-uptake experiment); then the spheroids are fished from the medium and are immersed in clear media (clearance) for another 24 h. The best fitting is illustrated in Fig. 6(d) for $D_{Ab} = (8.38 \pm 0.41) \times 10^{-12}$ m^2 s^{-1}. The uptake mass transfer coefficient is estimated as: $P_{Ab,\mathrm{up}} = (1.54 \pm 0.04) \times 10^{-9}$ m s^{-1}, and the release mass transfer coefficient of antibodies is computed: $P_{Ab,\mathrm{cl}} = (8.58 \pm 0.31) \times 10^{-9}$ m $\cdot$ s^{-1}.

To estimate the association, dissociation and internalization rate constants [k_{on}, k_{off}, k_{in}, see Eq. (6)], we fit

TABLE I. List of transport and reaction parameters for Rituximab and Trastuzumab antibodies. Comparison of computed antibodies transport and kinetic parameters with relevant literature.

Parameter	Fitting	Typical values
D_{Ab} ($\mu m^2\ s^{-1}$)	8.38 ± 0.41	5–50 [18–21]
$P_{Ab,up(cl)}$ ($m\ s^{-1}$)	2.5×10^{-10}–8×10^{-7}	3×10^{-9}–1.5×10^{-7} [22,23]
K_D (nM)	6.76 ± 1.75	1–10 (often in IgGs) [24]
k_{off} (s^{-1})	$(4 \pm 1.6) \times 10^{-3}$	10^{-6}–4×10^{-3} [24,25]
k_{int} (s^{-1})	$(1.4 \pm 0.57) \times 10^{-5}$	2×10^{-6}–2×10^{-4} [26–29]

the continuum-level model, Eqs. (6)–(9) on experimental measurements of the binding or specific antibody, the HER2-targeting Trastuzumab. Trastuzumab diffuses in the spheroid through the interstitium, and also associates (dissociates) on (from) the surface of cancer cells and internalizes; here, the porosity, ϕ_{Ab}, diffusion coefficient value, D_{Ab} and mass transfer coefficients, $P_{Ab,up(cl)}$, are adopted from the nonbinding antibody (Rituximab) experiments. The total concentration of antibody receptors, R_T is estimated from experimental measurements, and $R_T \approx 1060$ nM. The best fitting simulations of the Trastuzumab uptake and release experiments are illustrated in Fig. 6(e) for $k_{off} = (4 \pm 1.6) \times 10^{-3}\ s^{-1}$, $K_D \equiv k_{off}/k_{on} = 6.76 \pm 1.75$ nM (the equilibrium dissociation constant between the antibody and its antigen), and $k_{int} = (1.44 \pm 0.57) \times 10^{-5}\ s^{-1}$ (the internalization rate constant of the antibody). Our computed values for antibodies transport and kinetic parameters compare reasonably well with reported values in the relevant literature (see Table I).

ACKNOWLEDGMENTS

S.S. acknowledges the financial support of W. W. Smith Charitable Trust, the Allegheny Health Network-Johns Hopkins Cancer Research Fund, Maryland Innovation Initiative TEDCO. Y.K. was supported from the U.S. Air Force Office of Scientific Research, for AFOSR, the Award No. FA9550-21-0317.

[1] American association for cancer research. AACR Cancer Progress Report 2023, http:/https://cancerprogressreport.aacr.org/progress/.

[2] E. E. Vokes, Combined modality therapy of solid tumours, The Lancet **349**, S4 (1997).

[3] C. Zhu, M. Sempkowski, T. Holleran, T. Linz, T. Bertalan, A. Josefsson, F. Bruchertseifer, A. Morgenstern, and S. Sofou, Alpha-particle radiotherapy: For large solid tumors diffusion trumps targeting, Biomaterials **130**, 67 (2017).

[4] A. Howe, O. Bhatavdekar, D. Salerno, A. Josefsson, J. Pacheco-Torres, Z. M. Bhujwalla, K. L. Gabrielson, G. Sgouros, and S. Sofou, Combination of carriers with complementary intratumoral microdistributions of delivered α-particles may realize the promise for 225Ac in large, solid tumors, J. Nucl. Med. **63**, 1223 (2022).

[5] A. I. Minchinton and I. F. Tannock, Drug penetration in solid tumours, Nat. Rev. Cancer **6**, 583 (2006).

[6] A. Prasad, R. Nair, O. Bhatavdekar, A. Howe, D. Salerno, M. Sempkowski, A. Josefsson, J. Pacheco-Torres, Z. M. Bhujwalla, and K. L. Gabrielson, Transport-driven engineering of liposomes for delivery of α-particle radiotherapy to solid tumors: Effect on inhibition of tumor progression and onset delay of spontaneous metastases, Eur. J. Nuclear Med. Molec. Imag. **48**, 4246 (2021).

[7] S. Stras, T. Holleran, A. Howe, and S. Sofou, Interstitial release of cisplatin from triggerable liposomes enhances efficacy against triple negative breast cancer solid tumor analogues, Molecul. Pharmaceut. **13**, 3224 (2016).

[8] S. Stras, A. Howe, A. Prasad, D. Salerno, O. Bhatavdekar, and S. Sofou, Growth of metastatic triple-negative breast cancer is inhibited by deep tumor-penetrating and slow tumor-clearing chemotherapy: The case of tumor-adhering liposomes with interstitial drug release, Molec. Pharmaceut. **17**, 118 (2020).

[9] D. Salerno, A. Howe, O. Bhatavdekar, A. Josefsson, J. Pacheco-Torres, Z. M. Bhujwalla, K. L. Gabrielson, and S. Sofou, Two diverse carriers are better than one: A case study in α-particle therapy for prostate specific membrane antigen-expressing prostate cancers, Bioeng. Transl. Med. **7**, e10266 (2022).

[10] S. Karve, G. Bajagur Kempegowda, and S. Sofou, Heterogeneous domains and membrane permeability in phosphatidylcholine- phosphatidic acid rigid vesicles as a function of pH and lipid chain mismatch, Langmuir **24**, 5679 (2008).

[11] S. Karve, A. Alaouie, Y. Zhou, J. Rotolo, and S. Sofou, The use of ph-triggered leaky heterogeneities on rigid lipid bilayers to improve intracellular trafficking and therapeutic potential of targeted liposomal immunochemotherapy, Biomaterials **30**, 6055 (2009).

[12] R. R Nair, A. Prasad, O. Bhatavdekar, A. Sarkar, K. L. Gabrielson, and S. Sofou, Combined, yet separate: cocktails of carriers (not drugs) for α-particle therapy of solid tumors expressing moderate-to-low levels of targetable markers, Eur. J. Nuclear Med. Molec. Imag. **51**, 2649 (2024).

[13] A. K. Robertson, C. F. Ramogida, P. Schaffer, and V. Radchenko, Development of 225Ac radiopharmaceuticals: Triumf perspectives and experiences, Curr. Radiopharmaceut. **11**, 156 (2018).

[14] See Supplemental Material at http://link.aps.org/supplemental/10.1103/PhysRevResearch.6.033137 for (a) interstitial pH profile in spheroids, (b) dependence of liposomal drug release on pH, (c) dependence of drug uptake on pH, and (d) binding parameters for specific antibody with BT-474 cells.

[15] K. Fujimori, D. G. Covell, J. E. Fletcher, and J. N. Weinstein, A modeling analysis of monoclonal antibody percolation through tumors: A binding-site barrier, J. Nuclear Med. **31**, 1191 (1990).

[16] C. P. Graff and K. D. Wittrup, Theoretical analysis of antibody targeting of tumor spheroids: Importance of dosage for penetration, and affinity for retention, Cancer Res. **63**, 1288 (2003).

[17] G. M. Thurber, M. M. Schmidt, and K. D. Wittrup, Factors determining antibody distribution in tumors, Trends Pharmacol. Sci. **29**, 57 (2008).

[18] D. A. Berk, F. Yuan, M. Leunig, and R. K. Jain, Direct in vivo measurement of targeted binding in a human tumor xenograft, Proc. Natl. Acad. Sci. USA **94**, 1785 (1997).

[19] E. B. Brown, Y. Boucher, S. Nasser, and R. K. Jain, Measurement of macromolecular diffusion coefficients in human tumors, Microvasc. Res. **67**, 231 (2004).

[20] G. M. Thurber, M. M. Schmidt, and K. D. Wittrup, Antibody tumor penetration: transport opposed by systemic and antigen-mediated clearance, Adv. Drug Deliv. Rev. **60**, 1421 (2008).

[21] G. M. Thurber and K. D. Wittrup, Quantitative spatiotemporal analysis of antibody fragment diffusion and endocytic consumption in tumor spheroids, Cancer Res. **68**, 3334 (2008).

[22] M. R. Dreher, W. Liu, C. R. Michelich, M. W. Dewhirst, F. Yuan, and A. Chilkoti, Tumor vascular permeability, accumulation, and penetration of macromolecular drug carriers, J. Natl. Cancer Inst. **98**, 335 (2006).

[23] F. Yuan, M. Dellian, D. Fukumura, M. Leunig, D. A. Berk, V. P. Torchilin, and R. K. Jain, Vascular permeability in a human tumor xenograft: Molecular size dependence and cutoff size, Cancer Res. **55**, 3752 (1995).

[24] R. Schier, A. McCall, G. P. Adams, K. W. Marshall, H. Merritt, M. Yim, R. S. Crawford, L. M. Weiner, C. Marks, and J. D. Marks, Isolation of picomolar affinity anti-c-ErbB-2 single-chain Fv by molecular evolution of the complementarity determining regions in the center of the antibody binding site, J. Mol. Biol. **263**, 551 (1996).

[25] E. T. Boder, K. S. Midelfort, and K. D. Wittrup, Directed evolution of antibody fragments with monovalent femtomolar antigen-binding affinity, Proc. Natl. Acad. Sci. USA **97**, 10701 (2000).

[26] M. E. Ackerman, C. Chalouni, M. M. Schmidt, V. V. Raman, G. Ritter, L. J. Old, I. Mellman, and K. D. Wittrup, A33 antigen displays persistent surface expression, Cancer Immunol. Immunother. **57**, 1017 (2008).

[27] C. D. Austin, A. M. De Mazière, P. I. Pisacane, S. M. van Dijk, C. Eigenbrot, M. X. Sliwkowski, J. Klumperman, and R. H. Scheller, Endocytosis and sorting of ErbB2 and the site of action of cancer therapeutics trastuzumab and geldanamycin, Mol. Biol. Cell **15**, 5268 (2004).

[28] M. Jules Mattes, G. L. Griffiths, H. Diril, D. M. Goldenberg, G. L. Ong, and L. B. Shih, Processing of antibody-radioisotope conjugates after binding to the surface of tumor cells, Cancer **73**, 787 (1994).

[29] M. M. Schmidt, G. M. Thurber, and K. D. Wittrup, Kinetics of anti-carcinoembryonic antigen antibody internalization: Effects of affinity, bivalency, and stability, Cancer Immunol. Immunother. **57**, 1879 (2008).